



Research
Glycomedicine—Article

Absolute Quantification of Aging-Associated Glycans in IgG for Biological Age Prediction: Insights from Glycomics and Transcriptomics



Huijuan Zhao [#], Jiteng Fan [#], Jing Han, Wenjun Qin, Jichen Sha, Weilong Zhang, Yong Gu, Xiaonan Ma, Jianxin Gu ^{*}, Shifang Ren ^{*}

NHC Key Laboratory of Glycoconjugates Research, Department of Biochemistry and Molecular Biology, School of Basic Medical Sciences, Fudan University, Shanghai 200032, China

ARTICLE INFO

Article history:

Received 13 February 2025

Revised 27 July 2025

Accepted 31 July 2025

Available online 27 August 2025

Keywords:

Absolute quantification

Immunoglobulin G N-glycome

Aging

Glycan biomarker

ABSTRACT

Immunoglobulin G (IgG) N-glycans are associated with aging. In this study, we introduce a novel strategy for discovering aging-associated IgG glycans and establish a prediction model on the basis of their absolute concentration alterations. We employed glycomic quantification technology to identify alterations in the amount of IgG glycan in natural aging and antiaging (caloric restriction (CR)) models and discovered aging-related glycans. The glycomic analysis revealed key features: downregulation of the bisected glycan GP3 (F(6)A2B) and upregulation of the digalactosylated glycan GP8 (F(6)A2G2). These glycan changes showed significant fold changes from an early stage. Using external standards of these two glycans, we subsequently measured their absolute concentrations, allowing for us to establish a predictive model, abGlycoAge, for biological aging. The abGlycoAge index suggested a younger state under CR, with an average age reduction of 3.9–14.0 weeks. Additionally, RNA sequencing of splenic B cells revealed that *Derl3*, *Smarb1*, *Ankrd55*, *Tbkbp1*, and *Slc38a10* may contribute to alterations in GP3 and GP8 during the aging process. In a preliminary therapeutic study, we tested IgG modified with young signature N-glycans (IgG-Ny). High-dose IgG-Ny showed promising results, alleviating aging-related physiological declines, including reductions in inflammatory markers and improvements in organ senescence, particularly in the brain, kidney, and lungs. This research provides new insights into glycan changes during aging and lays the groundwork for potential antiaging therapies. GP3 and GP8 may serve as biomarkers for aging, offering new perspectives on aging mechanisms and therapeutic approaches.

© 2025 THE AUTHORS. Published by Elsevier LTD on behalf of Chinese Academy of Engineering and Higher Education Press Limited Company. This is an open access article under the CC BY license (<http://creativecommons.org/licenses/by/4.0/>).

1. Introduction

Aging induces complex physiological changes across multiple systems, making it essential to identify reliable biomarkers that can quantify these changes, explore the underlying mechanisms, and support the development of targeted interventions [1]. Among these changes, immunosenescence is a well-recognized feature that involves the gradual decline and imbalance of immune function, increasing the risk of infections, chronic inflammation, and cancer [2,3]. Recent research has focused on molecular biomarkers that reflect immunosenescence, including alterations in glycosylation patterns, especially immunoglobulin G (IgG), as these changes

have been linked to heightened inflammatory responses and immune dysfunction [4].

Glycosylation is a modification process of proteins and RNA, and there is also potential for glycosylations in DNA [5–7]. Glycosylation can significantly influence the biological activity and properties of these biomolecules. IgG glycans play crucial roles in modulating immune responses through various mechanisms. The glycosylation of IgG affects its effector functions, such as antibody-dependent cellular cytotoxicity (ADCC), complement activation, and Fc receptor binding [8,9]. These functions are essential for the clearance of pathogens and the regulation of immune responses. Studies have shown that IgG accumulates during aging in both mice and humans [10,11]. Moreover, the quantification of IgG N-glycans has shown promise in assessing biological age, with studies suggesting potential causal links between specific glycan structures and aging [12–16]. These findings demonstrate the potential of glycosylation as a biomarker for biological age and as

* Corresponding authors.

E-mail addresses: jxgu@shmu.edu.cn (J. Gu), renshifang@fudan.edu.cn (S. Ren).

[#] These authors contributed equally to this work.

a tool to explore age-related immune changes and guide therapeutic interventions.

However, while IgG *N*-glycan analysis has contributed significantly to understanding aging processes, current quantification techniques face limitations in fully defining aging-related glycan changes. Previous studies have primarily detected IgG *N*-glycans via high-performance liquid chromatography (HPLC) coupled with fluorescence detection, which quantifies each glycan as a proportion of the total glycan pool [14,15,17,18]. The relative quantification approach has been effective in identifying major changes across samples and has led to key discoveries, including aging-associated glycans, which have shown promise as biomarkers. However, the use of ratio values for assessment can introduce variability, complicating consistent interpretation across different samples and conditions [19]. In practical applications, absolute concentration measurements are often preferred, as they enable clear, standardized reference values suitable for diverse applications [20–23]. Furthermore, relative quantification may not adequately capture lower-abundance glycans that, while minor, may have biological significance in aging [19]. Therefore, absolute quantification [24,25] offers a complementary approach that enhances the applicability of glycan biomarkers by providing precise, direct measurements that reveal both major and subtle glycan changes.

Mass spectrometry (MS) is widely used for glycomic analysis because of its sensitivity, speed, and rich structural information through tandem MS approaches. However, the absolute quantification of glycans, particularly with matrix-assisted laser desorption/ionization time-of-flight mass spectrometry (MALDI-TOF-MS), remains challenging because of issues such as nonlinear signal response and the difficulty of finding suitable internal standards for diverse glycan structures [26]. Previous studies reported effective methods involving the use of three *N*-glycans and Malto-Series oligosaccharide standards or the chemoenzymatic synthesis of ¹³C-labeled *N*-glycan libraries to improve the accuracy of glycan quantification via MALDI-MS analysis [24]. Our laboratory previously developed a simple one-step method to obtain internal standards “Bionic Glycome” with full coverage of the natural *N*-glycome to be analyzed [27]. This method provides a unique solution to the challenges of glycan quantification by producing a structurally similar internal standard for each glycan, matched in abundance. This tailored internal standard approach minimizes interference from more abundant glycans, ensuring accurate detection even for low-abundance glycans that are often difficult to quantify with conventional methods. Moreover, this method enables the assessment of the amount alteration of each glycan, rather than the relative proportion in the total glycan pool, allowing for it to reveal absolute concentration changes across large sample sets. This capability is particularly valuable for identifying specific aging-associated glycans within complex glycan profiles. Once these specific glycans are identified, a standard curve can be established with an external standard glycan via the same MALDI-MS method, leveraging its speed and efficiency. By addressing the limitations of traditional MALDI-MS quantification, the approach in this study enables the development of biomarker models with precise, absolute measurements, which are essential for practical and reproducible biomarker applications.

Our prior work involved two studies on mouse aging and anti-aging effects. The aging study established an aging mouse model and examined changes in serum IgG *N*-glycans during aging, obtaining data on glycan abundance changes via HPLC quantification. The anti-aging study, which used a calorie-restricted model, explored overall serum *N*-glycan changes but did not focus on IgG *N*-glycans. Building on this foundation, the current study further explored the characteristics of IgG *N*-glycans during aging. We applied the Bionic Glycome method to analyze the IgG *N*-

glycans of C57BL/6 mice across different age groups, aiming to discover aging-associated glycans. Caloric restriction (CR) was used as an anti-aging intervention to further confirm the associations of these glycans with aging. We subsequently developed an absolute quantification method for aging-related glycans by using external glycan standards, enabling us to measure absolute concentration changes in these glycans across age and intervention groups. The predictive value of the model instructed with the absolute concentration in practical applications was also evaluated. To gain further insight, we integrated our glycan analysis with transcriptome analysis to examine gene expression patterns associated with aging. By comparing data from natural aging and anti-aging interventions, we identified several genes correlated with aging-related glycan changes, providing insights for future mechanistic studies. Additionally, to explore the therapeutic potential of IgG modified with young signature *N*-glycans (IgG-Ny) for reversing aging, we administered different doses of IgG-Ny or vehicle via tail vein injection to 80-week-old mice and evaluated various aging-associated biomarkers. This integrative approach not only enhances the utility of glycan biomarkers but also supports the development of predictive biomarkers and potential intervention strategies.

2. Materials and methods

2.1. Chemicals

Sodium dodecyl sulfate (SDS), 1-hydroxybenzotriazole monohydrate (HOBt), sodium borodeuteride (NaBD₄), trifluoroacetic acid (TFA), sodium hydroxide (NaOH), 2-aminobenzamide (2-AB), super-2,5-dihydroxybenzoic acid (super-DHB), Sepharose CL-4B, and ammonium bicarbonate (ABC) were purchased from Sigma-Aldrich (USA). 1-Ethyl-3-(3-(dimethylamino)propyl)-carbodiimide (EDC) hydrochloride was purchased from Fluorochem (UK). HPLC SupraGradient acetonitrile (ACN), ethanol (EtOH), and formic acid (FA) were obtained from Merck (Germany). Protein G Bestarose 4FF beads were purchased from Bestchrom (China). NP-40 and peptide-*N*-glycosidase F (PNGase F) were obtained from Adamas Life (China). The FiltrEX™ 96-well clear filter plate with a 0.2 μm polyvinylidene fluoride (PVDF) membrane was purchased from Corning (USA). Protein concentrations were determined via the Pierce™ BCA Protein Assay Kit (Thermo Fisher Scientific, USA).

2.2. Serum collection

Serum samples were collected from C57BL/6 mice aged between 23 and 80 weeks from both the aging (24–80 weeks) and anti-aging (23–60 weeks) studies [28,29]. These time points were selected on the basis of the established classification of aging stages in mice, which divides their lifespan into adulthood (12–26 weeks), middle age (27–56 weeks), and old age (≥ 56 weeks). Our preliminary HPLC studies revealed significant changes in the proportion of glycans starting at 24 weeks [28], indicating a critical transition point in the aging process. Therefore, we selected these time points to comprehensively investigate the alterations in the amount of IgG *N*-glycans across different stages of aging.

2.3. Analysis of IgG *N*-glycans

2.3.1. Analysis method design

We employed a quantitative strategy using the Bionic Glycome internal standard [22] to achieve absolute quantitation of the glycans. Briefly, glycans were extracted and purified from the analytes. A Bionic Glycome internal standard was added to each sample before analysis via MALDI-TOF-MS. The relative abundance of each glycan was determined by calculating the ratio between

the glycan analyte and the Bionic Glycome internal standard (Ratio 1 = analyte/internal peak intensity). Ratio 1 was used to identify characteristic glycans associated with aging. Characteristic glycans were then subjected to absolute quantitation. A series of known concentration characteristic glycans were used to quantify the characteristic glycans in the internal standard, yielding the ratio between the peak intensity of known concentration characteristic glycans and the peak intensity of characteristic glycans in the internal standard (Ratio 2 = known concentration glycans/internal peak intensity). An equation was established between Ratio 2 and concentration, and the concentration of the glycan analyte in the sample was calculated by substituting Ratio 1 into this equation. This quantitative strategy allows for us to avoid the need for known concentration internal standards for each individual glycan. Instead, we need to quantify only the internal standards for characteristic glycans.

2.3.2. Isolation of IgG from murine serum

IgG was isolated in a high-throughput manner via affinity chromatography as described previously [28]. In brief, murine IgG was captured from 30 μL of serum by Protein G Bestarose 4FF beads. Each serum sample was diluted 3-fold with 1 \times phosphate-buffered saline (PBS) and incubated with beads for 30 min. The beads were subsequently washed with PBS and nanopure water. IgG was eluted with 100 μL of 100 $\text{mmol}\cdot\text{L}^{-1}$ FA and neutralized with 1 $\text{mol}\cdot\text{L}^{-1}$ ABC. Studies have shown that IgG accumulates during aging in both mice and humans [10,11]. To exclude the influence of the protein concentration, each sample was adjusted to 25 μg and vacuum dried at room temperature.

2.3.3. Preparation of the released IgG N-glycans

Dried murine IgG samples were dissolved in 5 μL of water and 10 μL of 2% SDS and denatured for 10 min at 60 $^{\circ}\text{C}$. Then, 10 μL of glycobuffer (4% Nonidet P-40, 5 \times PBS, pH 7.5) and 1 μL of 10-fold diluted PNGase F were added to the mixture, followed by incubation at 37 $^{\circ}\text{C}$ for 16 h.

2.3.4. Preparation of the N-glycan internal standard

The Bionic Glycome of murine serum IgG was prepared as the internal standard [27]. The Bionic Glycome is composed of a set of deuterated hydroxyl forms of N-glycans that are similar in composition and abundance to those in the sample. The deuterated hydroxyl form of the N-glycan is generated through a one-step reduction process, which results in a mass difference of 3 Da compared with the hemiacetal form of the N-glycan present in the sample to be tested. Briefly, a mixture of mouse serum was prepared to isolate IgG and then release N-glycans. Once the volumes of EtOH and 1% FA were added, the mixture was incubated at 37 $^{\circ}\text{C}$ for 2 h. The N-glycans were subsequently reduced with 2 $\text{mol}\cdot\text{L}^{-1}$ NaBD₄ at 60 $^{\circ}\text{C}$ for 2 h.

2.3.5. Glycan enrichment and purification

Sepharose hydrophilic interaction chromatography solid-phase extraction (HILIC SPE) in a 96-well plate format was performed as described previously [29]. Specifically, N-glycan mixtures with acetonitrile were added to the activated Sepharose beads, and N-glycans were adsorbed to the beads. After three washes with 95% acetonitrile containing 1% TFA and three washes with 95% acetonitrile, the retained glycans were eluted with water, vacuum dried and stored at -20°C .

2.3.6. Sialic acid derivatization

Prior to MALDI-TOF-MS analysis, the samples were redissolved in 6.5 μL of water, and the internal standards were redissolved in 10.5 μL of water. Sialic acids are stabilized by ethyl esterification [30]. Two microliters of mixture from the sample or internal stan-

dards were added to 20 μL of esterification reagent (250 $\text{mmol}\cdot\text{L}^{-1}$ EDC hydrochloride and 250 $\text{mmol}\cdot\text{L}^{-1}$ HOBT monohydrate in ethanol) and incubated at 37 $^{\circ}\text{C}$ for 1 h. Cotton HILIC SPE microtips were used for microscale glycan purification and enrichment. Finally, the N-glycans were eluted in 10 μL of water.

2.3.7. Quantification of glycans

The N-glycan standards GP3 (F(6)A2B) and GP8 (F(6)A2G2) were obtained from the laboratory of Professor Tiehai Li (Shanghai Institute of Materia Medica, Chinese Academy of Sciences, China). First, a series of standard solutions with different concentrations were prepared to ensure coverage of the expected sample concentration range. The ratio of the target glycan to the Bionic Glycome internal standard in each standard solution was subsequently measured via MALDI-TOF-MS. These ratios were used to construct a linear standard curve, and the relationship between the target glycan concentration and the ratio was determined via linear regression analysis. Using these linear standard curves, we calculated the target N-glycan concentration in the eluate for each sample. Furthermore, we estimated the glycan content per gram of IgG for each mouse via the following formula:

$$G = C_{\text{Sample}} \times V_{\text{Dissolve}} \div V_{\text{EH}} \times V_{\text{EH_elute}} \div m$$

where G ($\text{nmol}\cdot\text{g}^{-1}$) is the glycan content per gram of IgG, C_{Sample} ($\text{nmol}\cdot\text{L}^{-1}$) is the N-glycan concentration of the sample in the eluate, V_{EH} is the volume of glycan used for ethyl esterification (2 μL), $V_{\text{EH_elute}}$ is the volume of water needed to elute the retained glycans (10 μL), V_{Dissolve} is the volume of water needed to redissolve the dried glycan (6.5 μL), and m is the amount of IgG used for analysis (25 μg).

2.3.8. MALDI-TOF-MS detection

The Bruker UltrafleXtreme laser (Bruker Daltonics, Germany) equipped with Smartbeam-II operated with the flexControl program (Bruker Daltonics) was used to detect the ethyl esterified IgG N-glycans. Each sample was mixed with an equal volume of the internal standard and 1 μL of the internal standard on a MALDI target (MTP 384 polished steel BC; Bruker Daltonics), with three duplicate dots per sample. After air drying, one microliter of 5 $\text{mg}\cdot\text{mL}^{-1}$ super-DHB in 50% ACN and 1 $\text{mmol}\cdot\text{L}^{-1}$ NaOH was added, and the spots were allowed to dry in air. The samples were measured in reflected positive ion mode. The mass window of m/z was set from 1000 to 3000. For each spectrum, 8000 laser shots were accumulated at a laser frequency of 1000 Hz via a complete random walk with 100 shots per raster spot.

2.3.9. MALDI-TOF-MS data processing and statistical analysis

The mass spectra were processed with flexAnalysis v3.4 (Bruker Daltonics). The acquired spectra were internally recalibrated via a set of calibration masses (1485.5337, 1647.5865, 1809.6393, 1982.7081, 2144.7609, and 2479.8826), and the glycan compositions were known (Table S1 in Appendix A). Masses were selected from the spectra via a sum algorithm, followed by quadratic calibration. A total of 20 pairs of glycans were identified (signal to noise threshold (S/N) > 3). The recalibrated spectra were imported into the BioPharma Compass software (Bruker Daltonics) to extract the peak intensity of each spectrum in batches. The analysis was performed as a target data extraction using a determined list of glycan compositions calculated as $[M + \text{Na}]^+$.

The relative abundance of each N-glycan (Ratio 1 = analyte/internal peak intensity) was used for quantification, and the interday and intraday repeatability of the glycans were examined. The total level of N-glycans was calculated by summing the relative abundance results of all the glycans.

The glycan structures were assigned via GlycoWorkbench (v 2.1). Data analysis and visualization were performed in R (v 4.3.3) via the following packages: readxl, dplyr, tidyr, rio, stringr,

tidyverse, ggplot2, and tidymodels. The differences among various age groups were assessed via one-way analysis of variance (ANOVA), followed by the Benjamini–Hochberg (BH) test procedure to adjust the *p* values for multiple comparisons. Unpaired *t* tests were used to compare differences in glycans between two groups at the same time point. A *p* value of less than 0.05 was considered statistically significant.

2.3.10. IgG N-glycan labeling, purification, and ultra performance liquid chromatography with fluorescence detection (UPLC-FLR) detection

IgG N-glycans were labeled with 2-aminobenzamide (2-AB) (Sigma-Aldrich, USA), purified via Sepharose HILIC SPE, and then analyzed via UPLC-FLR on a Nexera UPLC LC-30A system (Shimadzu, Japan) with a BEH amide column (Waters, USA). The FLR detector was set at an excitation wavelength of 330 nm and an emission wavelength of 420 nm. The 2-AB dextran ladder was used as an external standard for qualitative calibration.

2.3.11. UPLC-FLR data processing and statistical analysis

The assigned peaks in the UPLC chromatograms were selected to quantify the IgG N-glycans via LabSolution software. The relative abundance of each glycan was expressed as a percentage of the total integrated peak area. For statistical analysis, GraphPad Prism 8 was used. Unpaired *t* tests were used to compare differences in glycans between two groups at the same time point. A *p* value of less than 0.05 was considered statistically significant.

2.4. Splenic B-cell transcriptome analysis

Mouse CD19⁺ B cells were isolated from mouse spleen cell suspensions via a B-Cell Isolation LS Column and a MidiMACS[™] Separator (Miltenyi, Germany). Total RNA was extracted from these isolated B cells. The gene expression profiles were compared among three young mice (20 week), six aged mice (60 week) fed an *ad libitum* (AL) diet, and five aged mice (60 week) subjected to calorie restriction. Library construction and sequencing were performed on the Illumina platform provided by Novogene, China. The DESeq2 package (v1.20.0) [31] was used for identifying differentially expressed genes (DEGs), applying thresholds of $|\log_2(\text{fold change (FC)})| > 1$ and false discovery rate (FDR) < 0.05. Gene set enrichment analysis (GSEA) [32] was conducted with gsea (v4.3.2) for functional annotation of the gene expression profiles. The parameters were set as follows: permutation type = “permute phenotype,” metric for ranking genes = “signal2noise,” set_min = 15, and set_max = 5000; all other variables were set to default values.

IgG N-glycan-related DEGs were screened by integration of the union of DEGs across all possible combinations of the three groups; the genes associated with protein N-linked glycosylation (gene ontology (GO): 0006487) were retrieved from the Mouse Genome Database (MGD) [33], and the candidate genes were identified via previous genome-wide association studies (GWAS) [34–38]. The R package “biomaRt” (v2.60.0) was used to convert gene identities (IDs). Plots were produced via Origin 2021 (OriginLab, USA) and the R package “pheatmap” (v1.0.12).

2.5. IgG extraction from young mice

Blood was collected from 30–40-week-old anesthetized C57BL/6J mice and allowed to clot at room temperature for 2 h. The clotted blood was centrifuged at 3000g for 10 min, and the supernatant was collected. IgG was purified from the serum via a commercial IgG purification kit (Thermo Fisher Scientific). The purified IgG was then dialyzed against a 10 K molecular weight cut-off (MWCO) dialysis membrane and sterilized with a 0.22 μm sterile filter (Thermo Fisher Scientific).

2.6. IgG treatment of old mice

Eighty-week-old male wild-type C57BL/6J mice were administered self-extracted IgG-Ny or vehicle. IgG was mixed in PBS and administered to the mice via intravenous (i.v.) injection via the tail vein. Each group consisted of two mice, and 100 or 200 μg of IgG or vehicle was given to the mice four times weekly. The selection of these doses was informed by previous studies [39–41]. The doses and injection frequencies used were selected on the basis of previous studies demonstrating the efficacy of similar doses in different experimental models and considering the physiological characteristics of aged mice to ensure therapeutic effects while minimizing stress. At the end of the experiment, serum and tissue samples were collected for further analysis.

2.7. Cytokine analysis

The cytokines were estimated in the serum, which was separated and stored at –80 °C until the execution of the assay. The assay was conducted according to the manufacturer’s protocol via a Bio-Plex Pro Mouse Cytokine Grp I Panel 23-plex kit (#M60009RDPD; Bio-Rad Laboratories, USA) with a Luminex 200 system (Luminex Corporation, USA) at Wayen Biotechnology (China).

2.8. Senescence-associated β-galactosidase (SA-β-Gal) staining

SA-β-Gal staining was conducted in mouse tissues, including the brain, lung, liver, and kidney. Staining was performed according to the manufacturer’s protocol via a SA-β-Gal staining kit (Ab65351; Abcam, UK) at Wuhan Pinofly Biotechnology (China). Frozen sections were prepared via a HM525 NX cryostat (Thermo Fisher Scientific) and fixed in the kit’s fixation solution for 15 min at room temperature. The sections were washed, incubated with staining solution containing X-gal at 37 °C for 24 h, and counterstained with nuclear fast red for 3 min. After dehydration in ethanol and clearing in xylene, the sections were mounted with neutral gum. Images were captured via a digital camera attached to a microscope (Nikon, Japan) and analyzed via Image-Pro Plus 6.0 software (Media Cybernetics, Inc., USA).

3. Results

3.1. Age-related changes in IgG N-glycosylation patterns in C57BL/6 mice

IgG N-glycans from the aging cohort mouse sample (*n* = 89, 5 per sex at each time point) were analyzed via MALDI-MS via the Bionic Glycome method. The study design is illustrated in Fig. 1. A total of 20 glycans were observed, all of which had been previously identified via HPLC–fluorescence detection (FLR)–electrospray ionization (ESI)–time-of-flight mass spectrometry (TOF-MS) [28] or MALDI-TOF-MS [42], with a coefficient of variation (CV) of less than 20% in the reproducibility test (Fig. S1(a) and Table S1 in Appendix A). Additionally, four glycans (GP10+GP11, GP13, GP15, and GP16) that contained both α2,3- and α2,6-linked sialic acids were combined in the subsequent quantitative calculations to ensure comparability with previous HPLC results [28]. Therefore, a total of 14 glycans with the same glycan ID as those in our previous HPLC results [28] were further analyzed (Fig. S1(b) and Table S1 in Appendix A).

The results revealed a general trend of increased IgG N-glycosylation early in life, followed by a decrease during aging (Fig. 2(a), Fig. S2 in Appendix A). In male mice, IgG N-glycosylation levels initially increased slightly with age before

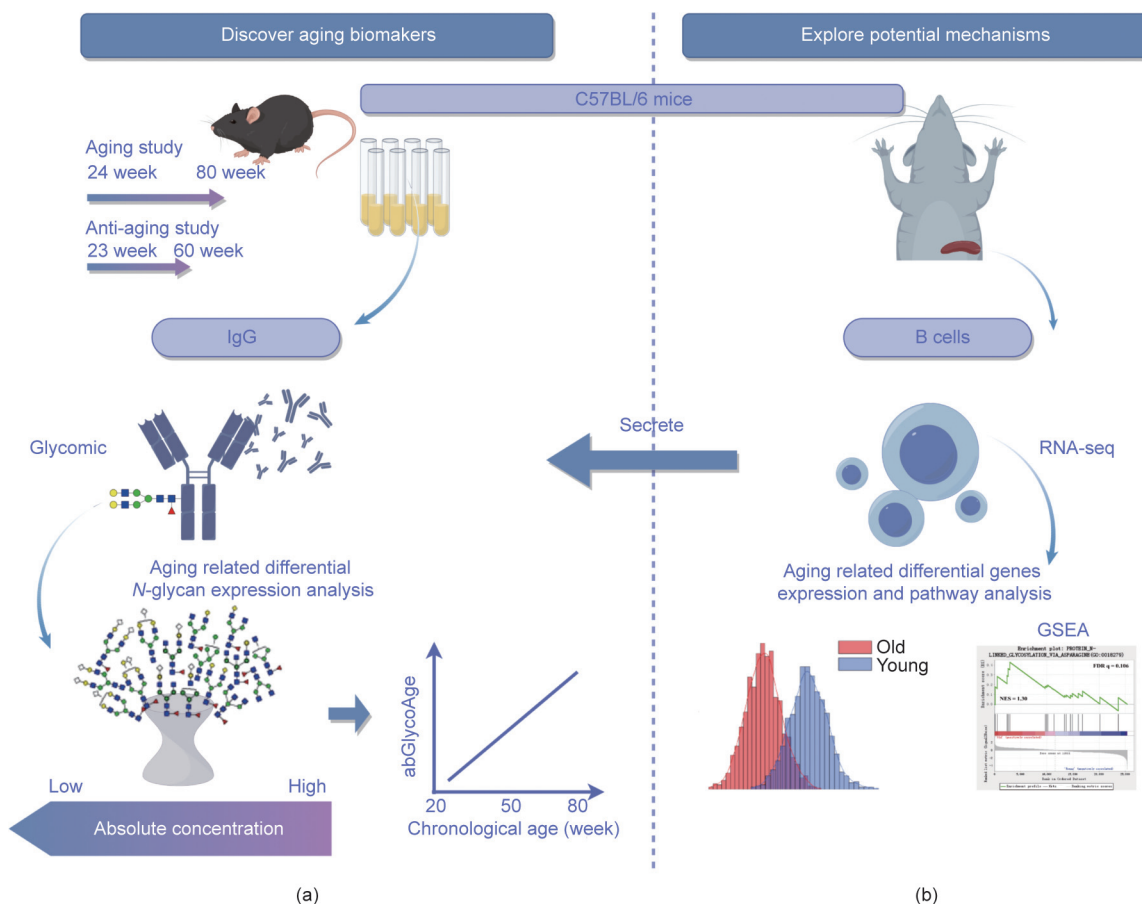


Fig. 1. Study design for predicting biological age from aging-associated glycans in IgG by integrating glycomics and transcriptomics. We performed a comprehensive IgG N-glycome profiling in C57BL/6 mice at seven time points across 80 weeks by MALDI-TOF-MS. Alterations in glycan amount were detected using an internal full-glycome standard. By referencing exogenous standards, we introduced a novel method for detecting aging biomarkers based on their absolute concentration. Based on the absolute concentrations of aging-related IgG glycans, we established abGlycoAge index to evaluate the biological age and applied in anti-aging assessment. The potential molecular basis of these IgG aging-related glycans was explored by splenic B cell transcriptome. RNA-seq: RNA sequencing.

declining at 68 weeks, although this change did not reach statistical significance. In female mice, IgG N-glycosylation levels also increased modestly with age before a highly significant decrease occurred at 80 weeks (Fig. S2). Correlation analysis revealed sex-specific differences in age-related glycan changes: in males, six glycans (GP1, GP4+GP5, GP7, GP8, GP9, and GP14) were positively correlated with age, whereas GP3 was negatively correlated. In females, three glycans (GP4+GP5, GP8, and GP14) were positively correlated with age, whereas four (GP2, GP3, GP6, and GP10+GP11) were negatively correlated (Figs. 2(b) and (c)). Compared with 24-week-old mice, both male and female mice presented significant FCs in the expression of GP3 and GP8 at multiple time points (Fig. 2(d)). On the basis of these findings, we identified the key aging-associated glycans in C57BL/6 mice as downregulated GP3 (F(6)A2B) and upregulated GP8 (F(6)A2G2) (Fig. 2(e)).

3.2. CR reverses key age-related IgG N-glycan changes in C57BL/6 mice

We then performed quantitative analysis of individual IgG N-glycans in CR and AL mice. The results revealed a general trend of increased IgG N-glycosylation in CR mice (Fig. 3(a)). Although GP3 expression still gradually decreased with age after CR, its expression level remained higher in CR mice than in age-matched AL mice. Notably, the changes in GP3 diminished after long-term CR, likely due to its low relative abundance (Figs. 3(b) and (c)). Additionally, glycans containing LacNAc structures, such as GP4+GP5 and GP8, displayed opposite trends after CR. Despite

the gradual increase in GP8 with age after CR, its expression level remained lower in CR mice than in age-matched AL-fed mice (Figs. 3(b) and (c), Fig. S3 in Appendix A). In summary, CR effectively reversed the age-related downregulation of GP3 (F(6)A2B) and the upregulation of GP8 (F(6)A2G2) in C57BL/6 mice.

We also detected changes in IgG N-glycans via UPLC-FLR after 2-AB labeling for comparison with previous studies [28]. The relative abundance of each glycan is expressed as a percentage of the total integrated peak area. We observed significant changes in the composition of 14 IgG glycans during the early stages of CR (15–35 weeks). Specifically, four N-glycans—GP2, GP3, GP6, and GP10+GP11—showed steady increases across all age groups, whereas GP4+GP5, GP8, and GP13 steadily decreased. Further analysis of IgG glycan expression in the serum of 60-week-old CR and AL mice revealed that the changes in GP2, GP3, and GP13 disappeared, with the CR group showing similar levels to those of the AL group. However, glycans containing LacNAc structures, such as GP4+GP5, GP8, and GP10+GP11, maintained their early-stage trends, continuing to either decrease or increase (Fig. S4 in Appendix A).

3.3. Development of a glycan-based biological age prediction model

In both male and female mice, GP3 and GP8 were significantly correlated with age, whereas the correlation between these two glycans was relatively weak (Pearson correlation coefficient ($|r|$) < 0.5). On this basis, we aimed to develop a glycan-based

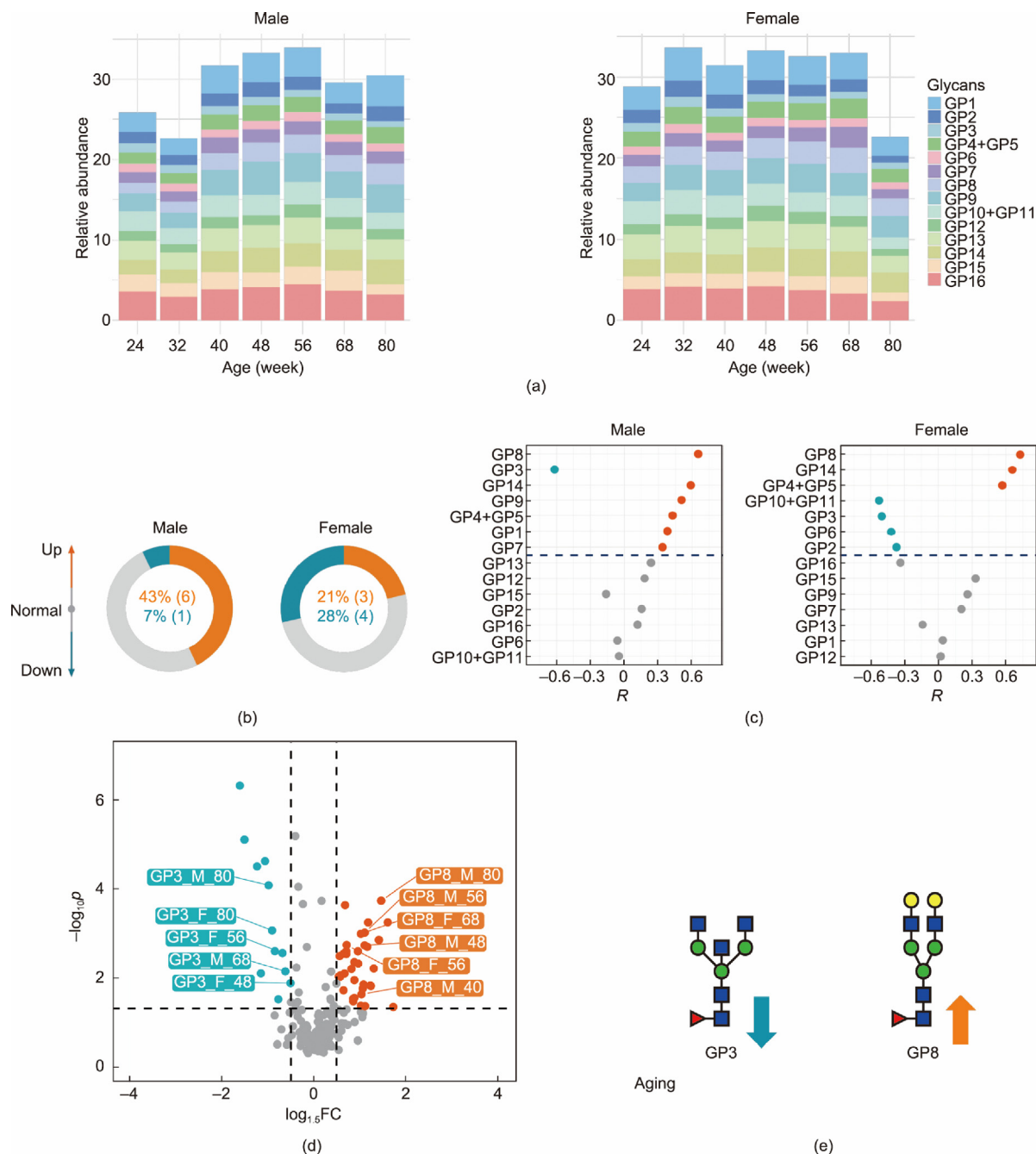


Fig. 2. Age-related changes in IgG N-glycosylation patterns in C57BL/6 mice at seven time points (24, 32, 40, 48, 56, 68, and 80 weeks). (a) Stacked bar chart illustrating the age-related changes in IgG total N-glycomes (each color representing a distinct glycan). (b) Schematic comparison of glycan alteration in aging. Circles show the percentage of glycan that are positively correlated with age (orange), negatively correlated with age (green), and no correlation (gray). (c) Dot plots show the correlation of each glycan with age. (d) Volcano plot show the FCs ($\log_{15}FC$) of glycan expression compared to 24-week-old mice. The differences among various age groups were assessed using the one-way ANOVA, followed by BH test procedure to adjust the p -values for multiple comparisons. Adjusted p values < 0.05 was considered to be statistically significant. F: female; M: male. (e) Schematic diagram highlights the crucial roles of the GP3 and GP8 as potential biomarkers for aging and health.

biological age prediction model using GP3 and GP8. First, we performed absolute quantification of the GP3 and GP8 ratio via standard glycans. Both glycans exhibited linear standard curves across the sample concentration range, with correlation coefficients (R^2) exceeding 0.999. The absolute concentration ranges were $1\text{--}25\text{ nmol}\cdot\text{L}^{-1}$ for GP3 and $100\text{--}500\text{ nmol}\cdot\text{L}^{-1}$ for GP8 (Figs. 4(a) and (b)). Using these linear standard curves, we calculated the glycan content per gram of IgG for each mouse (Fig. 4(b)) and fitted a model for predicting biological age on the basis of the absolute glycan content in mice of different ages (Fig. 4(c)).

Both GP3 and GP8 were strongly correlated with age in male and female mice, and their correlations with each other were weak ($|r| < 0.5$). On the basis of these glycan profiles, we developed a biological age prediction model, abGlycoAge, via absolute quantification of GP3 and GP8. The model explained 67% of the actual age variance in male mice and 57% in female mice, with correlations of 0.79 in males and 0.73 in females. When applied to predict biological age in CR cohorts, the model estimated that CR reduced biological age by an average of 14.0 weeks in males and 3.9 weeks in females, a reduction maintained throughout the lifespan (Fig. 4(d)).

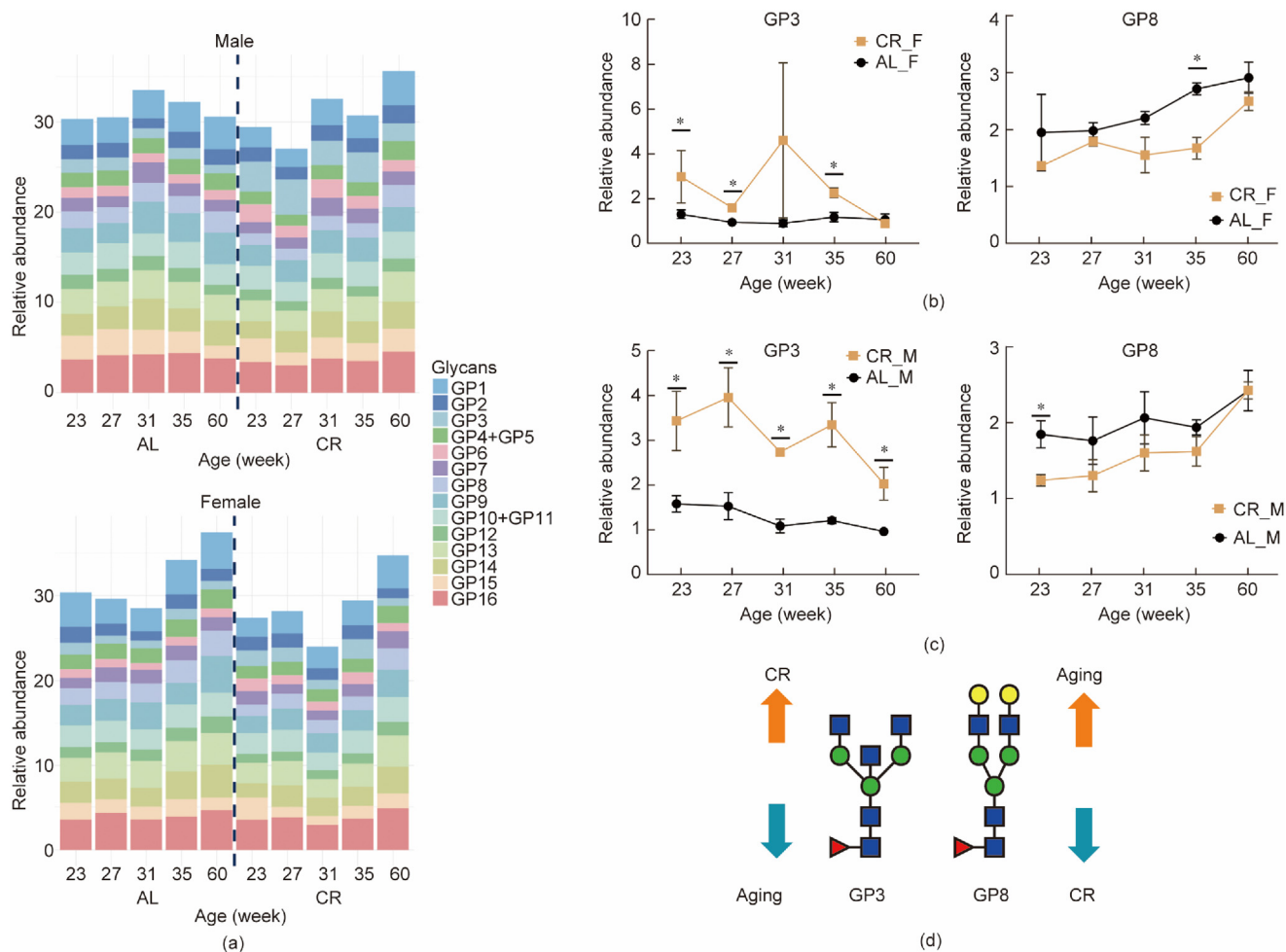


Fig. 3. CR reverses key age-related IgG glycan changes in C57BL/6 mice. (a) Stacked bar chart illustrate the age-related changes in IgG total N-glycomes both in AL and CR group (each color representing a distinct glycan). (b, c) Schematic comparison of glycan alteration in (b) female (F) and (c) male (M) in AL and CR groups (mean \pm standard error (SE)). The differences between AL and CR were assessed using the *. p values < 0.05 was considered to be statistically significant. * $p < 0.05$. (d) Schematic diagram highlights the crucial roles of the GP3 and GP8 as potential biomarkers for aging.

3.4. Mechanistic exploration: transcriptomic analysis of splenic B cells

A total of 7440 DEGs were observed in the comparisons among the three groups. Compared with those in young mice, 3114 DEGs were observed in aged mice, with 1782 upregulated and 1332 downregulated. GSEA revealed significant enrichment of the “protein N-linked glycosylation via asparagine” pathway (GO: 0018279) in aged mice, suggesting that protein N-glycosylation is upregulated during aging and that this effect is mitigated by CR (Fig. 5(a)).

IgG N-glycan-related DEGs related to the aging process were screened to elucidate the potential mechanisms underlying the changes in the expression levels of the aging biomarkers GP3 (F(6)A2B) and GP8 (F(6)A2G2). Candidate genes were pinpointed by synthesizing data from RNA sequencing (RNA-seq) analyses, the GO term for protein N-linked glycosylation (GO: 0006487) (Table S2 in Appendix A), and prior GWAS (Table S3 in Appendix A). Although these genes are known to be associated with N-glycosylation and IgG glycans, their expression level changes during aging have not been fully studied. As depicted in Fig. 5(b), among the 51 candidate genes, two genes were common across all three datasets, 24 were found in both the GO and DEG sets, and 25 were shared between the GWAS and DEG sets. The two common genes were *Der13* and *Fut8*. Most of the N-glycans were core fucosylated in mouse IgG, with the exceptions of GP7

(H6N2) and GP15 (H5N4G1Ge1 and H5N4Ge2). Therefore, the change in *Fut8* during aging appears to influence the level of total fucosylated N-glycans (Fig. S5 in Appendix A). The *Smarcb1–Der13* locus was previously implicated at the level of fucosylated structures with bisecting N-acetylglucosamine (GlcNAc) N-glycans of human IgG [34]. Our research has extended these findings by demonstrating that the expression of these two genes changes with age and can be reversed by antiaging interventions, thereby providing additional evidence for the mechanisms underlying the alterations observed in GP3 (F(6)A2B). *Fut8* is an essential α -1,6-fucosyltransferase gene that promotes core fucosylation. *Runx3*, which has been reported to regulate IgG glycosylation *in vitro*, was also upregulated in aged mice in our study but was restored in antiaging mice. Another group of genes included *Ankrd55*, *Tbkbp1*, and *Slc38a10*, which influence the percentage of agalactosylated and digalactosylated structures in total neutral IgG glycans (Table S2) [34,35]. This may be the basis for the alterations observed in GP8 (F(6)A2G2) (Fig. 5(c)).

3.5. Rejuvenation effect of IgG-Ny treatment

IgG is an aging factor that accumulates in various tissues during the aging process, leading to adipose tissue fibrosis, metabolic decline, and a significant enhancement of the senescence phenotype [10,11,43]. To verify the role of glycans, we hypothesized that

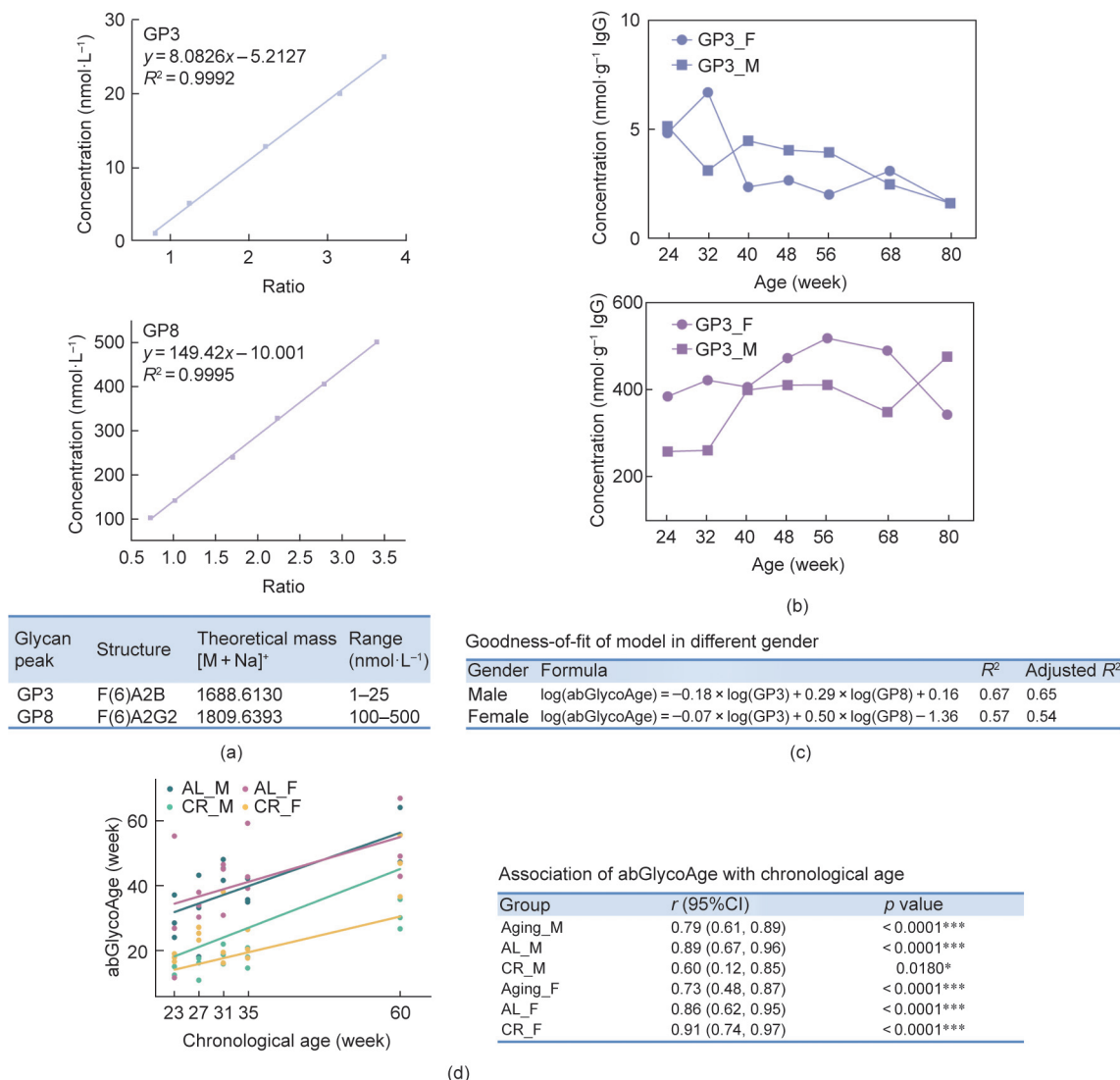


Fig. 4. Development the glycan-based biological age prediction model and assessment biomarker sensitivity in anti-aging study. (a) Absolute quantification of GP3 and GP8 was performed using standard glycans. The linear standard curves for both glycans exhibited correlation coefficients (R^2) greater than 0.999 across the sample concentration ranges of 1–25 nmol·L⁻¹ for GP3 and 100–500 nmol·L⁻¹ for GP8. (b) Glycan content per gram of IgG was calculated for mice in each age group based on the standard curves. (c) A model was fitted to predict biological age (abGlycoAge) using the absolute glycan content in mice of different ages. (d) The model predicted a sustained reduction in biological age in CR cohorts. *r*: Pearson correlation coefficient; CI: confidence interval; F: female; M: male.

supplementing a certain amount of IgG-Ny could counteract the pro-aging effects of IgG. We administered different doses of IgG-Ny or vehicle via tail vein injection to 80-week-old mice and then evaluated various aging-associated biomarkers (Fig. 6(a)).

We observed that all the mice in the control group survived throughout the entire experiment, whereas one mouse in the low-dose IgG-Ny group died after the last treatment. Interestingly, no mice died in the high-dose IgG-Ny group (Fig. 6(b)). Some phenotypic changes were observed: the low-dose IgG-Ny group mice presented relatively sparse black fur with some exposed skin, a slender body, and a reduced body weight, whereas the high-dose IgG-Ny group mice presented dense black fur and a body weight similar to that of the control group (Figs. 6(c) and (d)). The levels of the inflammatory cytokines interleukin-6 (IL-6) and tumor necrosis factor- α (TNF- α) were consistent with the observed phenotypic changes. After treatment with high-dose IgG-Ny, the levels of IL-6 and TNF- α in aged mice decreased, approaching or even dropping below those of the control group (Figs. 6(e) and (f)). This finding indicates that the dosage may have an effect on the rejuvenation effect.

We next investigated the impacts of IgG-Ny treatment on vital organs, such as the brain, lung, liver, and kidney. We measured the levels of SA- β -Gal in these vital organs (Figs. 6(g) and (h)). The data showed that in the low-dose IgG-Ny group, the mean density of SA- β -Gal in the lungs and kidneys increased, whereas it decreased in the high-dose IgG-Ny group. Notably, even in the low-dose IgG-Ny group, the mean density of SA- β -Gal in the brain decreased significantly, indicating a high sensitivity of the brain to IgG-Ny treatment. In contrast, the impact of the IgG-Ny treatment on the liver was relatively minor. These findings indicate that different organs may exhibit heterogeneity in their responses to IgG-Ny treatment.

4. Discussion

Glycans are valuable biomarkers because of their stability and ability to integrate genetic, epigenetic, and environmental factors into quantifiable chemical structures, making them ideal for personalized medicine [44]. Recent research has highlighted the significant role of α 2,6-sialylation in the occurrence of Alzheimer's

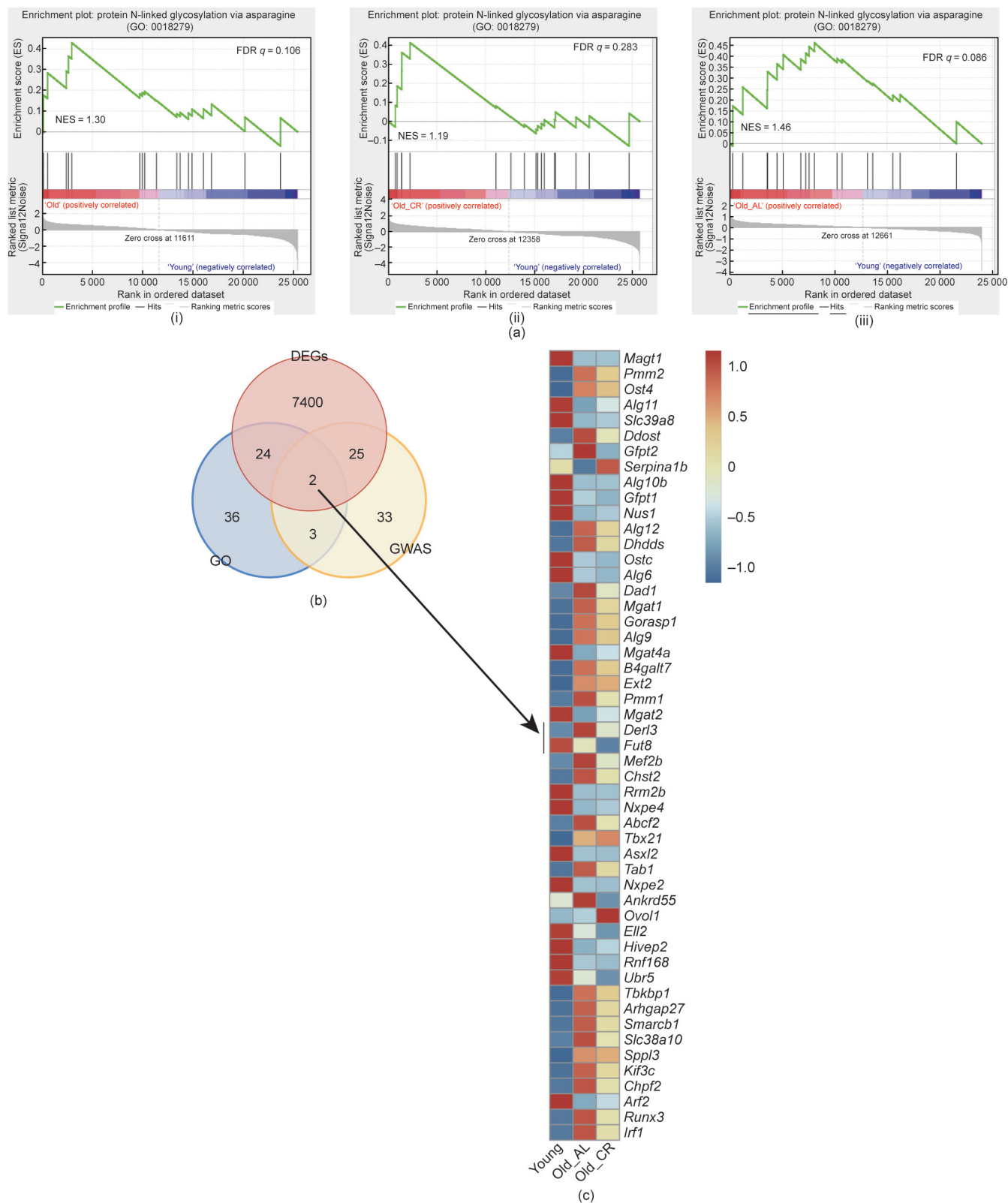


Fig. 5. IgG N-glycan-related genes and pathway perturbation as potential mechanisms underlying variations in glycosylation phenotypes during aging. (a) GSEA plots illustrating the activation of “protein N-linked glycosylation via asparagine” in aged mice across various comparisons: (i) old vs young, (ii) old_CR vs young, and (iii) old_AL vs old_CR. NES: normalized enrichment score; q : false discovery rate (FDR) q -value. (b) Venn diagram illustrating the IgG N-glycan-related DEGs identified through by integration of transcriptome analysis, GWAS, and GO terms. DEGs identified via transcriptome analysis, encompassing the union of DEGs across all possible combinations of the three groups. GWAS: genes identified in previous genome-wide association studies; GO: genes associated with protein N-linked glycosylation (GO: 0006487). (c) The expression patterns of IgG N-glycan-related DEGs for three group (20 weeks for young, 60 weeks for old_AL and old_CR) was shown in the left heatmap.

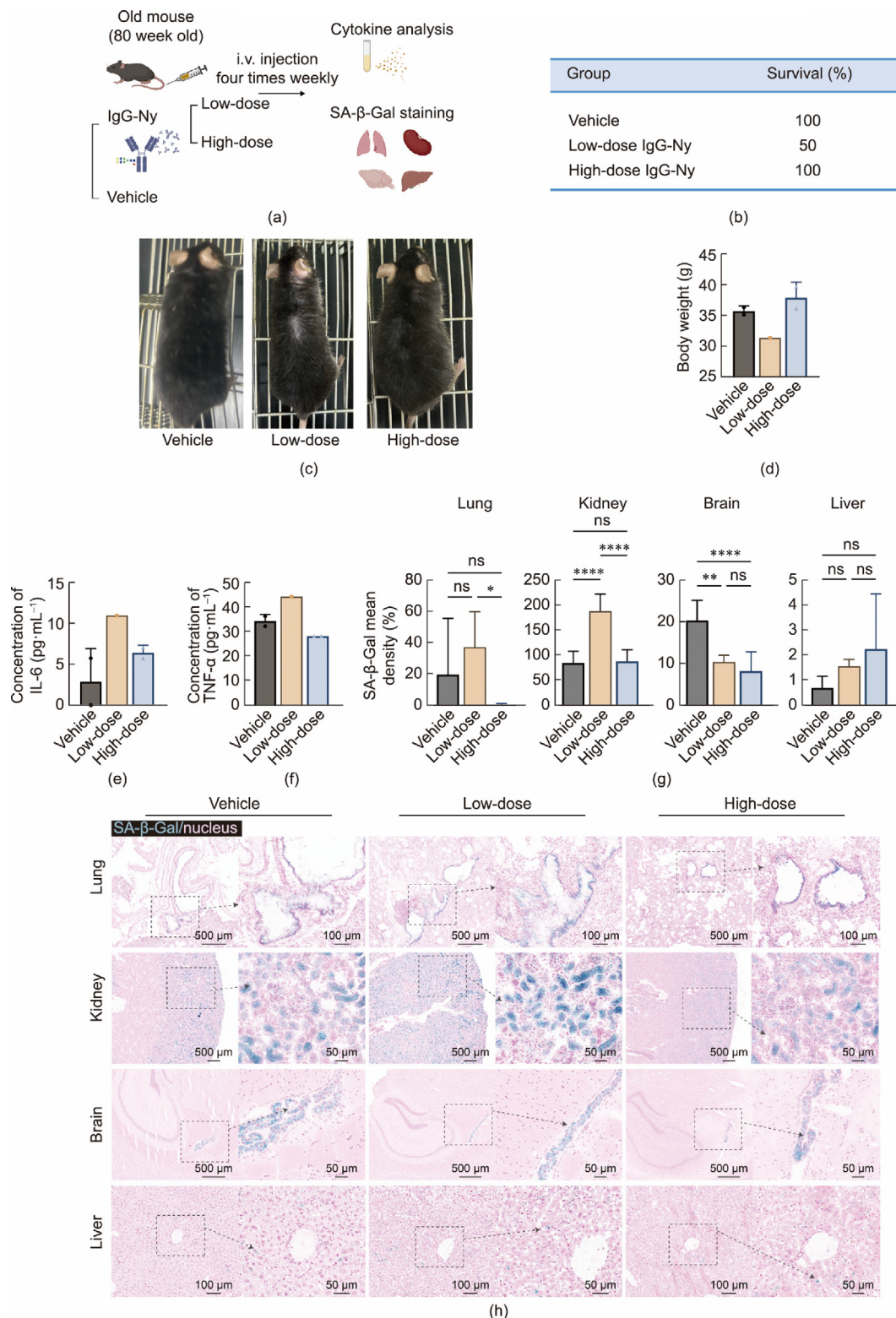


Fig. 6. IgG-Ny treatment ameliorated the multi-tissue aging in male mice. (a) A schematic illustrating the treatment of 80-week-old mice with IgG-Ny or vehicle. Image created with bioRender. (b) The survival rate, (c) representative images, and (d) body weight of mice before being sacrificed. Blood levels of (e) interleukin-6 (IL-6) and (f) tumor necrosis factor- α (TNF- α) were measured and data are presented as the mean \pm standard deviation (SD). (g) The mean density and (h) representative images of SA- β -Gal staining of the lung, kidney, brain, and liver from old mice treated with IgG-Ny or vehicle. Five representative high-power visual fields were selected to calculate the mean density of SA- β -Gal in each group. One-way ANOVA with Tukey's multiple comparison was utilized for the data in (g), and data are presented as the mean \pm SD. The arrows indicate positive area. * $p < 0.05$; ** $p < 0.01$; **** $p < 0.0001$; ns: no significance.

disease (AD), suggesting that $\alpha 2,6$ -sialyltransferase-I (ST6Gal-I) is a novel glycan therapeutic target for AD diagnosis and treatment [45]. To facilitate the translation of such glycosylation-related tar-

gets into clinical applications, a deeper understanding of the specific glycan compositions and their quantitative alterations would be highly beneficial.

Aberrant N-glycosylation modulates IgG effector functions flexibly and dynamically, with aging driving a shift in the IgG N-glycome from an anti-inflammatory to a proinflammatory composition [46]. These changes in glycan composition are often reflected in specific glycan levels. Previous studies have demonstrated that relative quantification is an effective approach for assessing glycosylation changes [14,28]. However, examining glycan changes from an absolute quantification perspective is more suitable for the practical application of glycans as biomarkers [19,47]. In clinical applications, widely used biomarkers such as cancer antigen 125 (CA-125) and prostate-specific antigen (PSA) in tumor screening [21], metabolites in newborn screening [23], and cyclosporin A (CsA) levels in blood for managing immunosuppression after organ transplantation [20] all depend on absolute quantification. This study offers valuable insights into specific glycan shifts associated with aging by focusing on their absolute concentrations. The capacity to measure biological aging through glycans holds significant potential for practical applications, including the evaluation of aging processes and the effectiveness of anti-aging interventions.

To our knowledge, this is the first longitudinal study to provide detailed information on the absolute concentration changes in IgG glycan levels in mice. In recent years, the continuous development of new technologies has been remarkable, with significant advancements in high-throughput sample processing, multiglycosylation-omics analysis, and the identification of low-abundance glycopeptides. For example, the emergence of the GlycoPro platform has provided a high-throughput sample-processing solution for multiglycosylation-omics analysis [48]. In terms of low-abundance glycopeptide identification, the innovative N-glycoproteomic workflow developed by Zuniga-Banuelos et al. [49] has significantly enhanced the detection of low-abundance glycoproteins in human blood plasma by integrating protein depletion, fractionation strategies, and high-resolution MS. This workflow not only enables the detection of glycoproteins with reported concentrations at the nanogram per milliliter level but also significantly improves the description of N-glycan microheterogeneity through a newly developed decision tree procedure. This advancement allows for researchers to reliably differentiate ambiguous N-glycan structures such as antenna versus core fucosylation, as well as identify rare and modified N-glycans such as sulfated and glucuronidated ones. The development of absolute quantification methods still requires further acceleration to improve the analytical speed and efficiency. In this study, we employed a simple, rapid and reliable method based on MALDI-TOF-MS to assess alterations in the amount of IgG glycan, which significantly improved both the experimental efficiency and the data accuracy. In addition to natural aging, we included CR as an antiaging intervention, enabling a comprehensive analysis of IgG N-glycosylation patterns and offering new perspectives on the antiaging mechanism. With over 100 samples and multiple time points, our study provides a robust and comprehensive dataset. The large sample size and detailed temporal profiling enhance the reliability of our results, offering valuable insights into glycan changes over time.

Previous studies have reported that total IgG concentrations may vary with age [10,11]. Aging and age-related diseases, such as cardiovascular diseases and hypertension, have also been shown to affect the serum and plasma IgG glycan profiles [14,15,50]. For example, GlycanAge and GlycanBioAge are biomarkers based on the analysis of glycans, which can more accurately predict chronological and biological ages and provide potential tools for the assessment of individual health status and the aging process [14]. GlyCage is a novel biomarker based on two bisecting N-glycans of IgG, which can more accurately predict cardiovascular risk and provides a potential tool for the early screening of cardio-

vascular diseases (CVDs) [50]. However, most existing studies have focused on relative quantification, assessing glycans in terms of their proportions within the total glycan pool. While this approach has provided important insights into age-related glycan changes, it does not capture absolute abundance shifts that may carry additional biological significance. Our method enables absolute quantification of specific glycans, offering complementary information to relative profiling and demonstrating improved applicability in aging-related research. Characteristic age-related glycan changes were observed in IgG, and the concentrations of these characteristic glycans were expressed as nanomoles per gram of IgG. In this study, we identified two main N-glycans in C57BL/6 mouse serum IgG from 24 to 80 weeks. The downregulation of GP3 (F(6)A2B) and the upregulation of GP8 (F(6)A2G2) are significant characteristics of aging in these mice. To our knowledge, galactosylation levels in human plasma IgG have shown the strongest association with age [12–14]. Despite species-specific differences leading to divergent trends, in our study, we observed age-related changes in the serum IgG levels of GP8 (F(6)A2G2), a glycan with two galactoses, in C57BL/6 mice, both in terms of relative [28] and absolute quantification. These findings highlight GP8 as an important hallmark of aging. Since GP8 is a glycan with a digalactosylated structure, this structural characteristic makes it more susceptible to regulation by estrogen [51]. Our research also revealed that, compared with that in male mice, the expression level of GP8 in female mice was more strongly correlated with age. These findings suggest that the sex-specific differences in IgG glycans during aging may be related to the regulation of IgG N-glycosylation by sex hormones.

In previous studies, bisecting N-acetylglucosamine (GlcNAc) glycans were detected in both mouse and human IgG [14,15,17,18,42]. However, findings regarding the association between bisecting GlcNAc glycans and aging in mice have been inconsistent, likely due to the limitations of relative quantification methods. These studies primarily employed HPLC with fluorescence detection, which quantifies glycans on the basis of their relative proportions in the total glycan pool. This relative quantification approach is particularly limited when characterizing low-abundance glycans, such as GP3 (F(6)A2B), as their measurement can be significantly influenced by the presence of high-abundance glycans. In contrast, the use of absolute quantification allows for a more comprehensive understanding of bisecting GlcNAc changes during mouse aging, providing clearer insights into the age-related significance of this glycan. Notably, both the GP3 and GP8 levels were modulated by calorie restriction. These findings suggest that calorie restriction may delay the aging process by stabilizing GP3 expression and suppressing GP8. However, further mechanistic studies are needed to determine whether these glycosylation changes in IgG are a cause or a consequence of reduced inflammation following CR.

Transcriptomic analysis of splenic B cells was integrated to enhance our understanding of the relationship between the observed aberrant specific glycan levels and aging. To our knowledge, we have, for the first time, unveiled the RNA-seq landscape of splenic B cells within the context of aging, which includes both the natural aging process and the state following antiaging interventional measures. Previously, GWAS [34–38] identified genetic variants linked to specific glycan traits; however, their impact on gene expression has rarely been investigated. In addition, the composition ratios of specific glycans obtained via traditional methods are technically difficult to directly correlate with the expression profiles of genes. Our method revealed changes in the amount of glycan, which can theoretically correlate better with gene expression alterations, providing insight into the underlying mechanism of glycan alterations.

We focused on genes related to N-glycan synthesis, as well as the 63 genes associated with IgG glycosylation reported in

previous GWASs [34–38]. We observed the activation of key pathways regulating the synthesis of IgG *N*-glycans through “protein *N*-linked glycosylation via asparagine” pathway. Given that we used 60-week-old mice for transcriptome analysis, these findings are in line with the observed increase in total *N*-glycan levels in aged mice younger than 68 weeks (Fig. 2(a), Figs. S2(a) and (b)). Additionally, we identified changes in the expression levels of 27 out of the 63 genes associated with IgG glycosylation as reported by the GWAS, with three of these genes (*Hivep2*, *Sppl3*, and *Runx3*) also previously validated through *in vitro* experiments for their correlation with IgG glycan expression levels, which indicates the reliability of our findings. Furthermore, we provide evidence that the expression levels of the other 24 genes may also regulate IgG glycosylation *in vivo*. We further validated the associations of these genes with aging by investigating whether alterations in gene expression during natural aging can be reversed in an antiaging model.

Among them, five genes were previously found to be associated with bisected glycans and galactosylated glycans [34,35]. Bisecting and galactosylation are also the main traits of GP3 and GP8, respectively. These findings suggest that *Derl3* and *Smarb1* might be the main contributors to the alteration of GP3. Similarly, *Ankrd55*, *Tbkbp1*, and *Slc38a10* might be the main contributors to the alteration of GP8. Among them, *Derl3* is a promising functional candidate gene because it encodes a functional component of the endoplasmic reticulum (ER)-associated degradation pathway, which specifically targets misfolded glycoproteins [34]. These findings suggest that *Derl3* may indirectly influence the glycosylation of IgG by affecting the folding and degradation processes of glycoproteins within the ER. Our research reveals their expression characteristics *in vivo* and, through aging and antiaging studies, suggests that these genes may constitute the main molecular basis for the IgG glycans GP3 and GP8 during the aging process.

Finally, we investigated the effects of supplementation with a certain amount of IgG-Ny on aging-related biomarkers and organ functions. The results revealed the potential role of IgG-Ny treatment in reversing aging, as well as its dosage dependence and organ heterogeneity. In our results, high-dose IgG-Ny failed to promote aging. Conversely, the high-dose IgG-Ny-treatment effectively improved the accumulation of pro-aging IgG, thereby alleviating aging-related physiological decline, reducing the production of aging-related inflammatory factors, and more effectively clearing senescent cells or inhibiting their accumulation to improve organ functions, particularly in the brain, kidney, and lungs. The results showed that the brain is highly sensitive to IgG-Ny treatment, suggesting a new perspective for understanding the treatment of aging-related diseases such as cognitive impairment and AD. These results indicate that IgG-Ny treatment has the potential to reverse aging, but its effects are dosage-dependent and organ-specific.

The current study has several limitations that should be acknowledged. We did not include body weight or fat mass as covariates in our primary aging analysis, as all the mice were maintained under consistent dietary and housing conditions, and differences in these parameters were largely age-driven rather than reflecting independent sources of variation. Moreover, changes in body composition are recognized features of the aging process. Adjusting for these factors may obscure biologically relevant trends directly linked to age. Notably, in the IgG-Ny intervention experiment, we incorporated body weight as a phenotypic indicator and observed trends consistent with improvements in inflammatory status and organ senescence. In future work, we plan to systematically monitor body weight and fat mass to further investigate their relationships with changes in IgG glycosylation. As an exploratory attempt, we conducted a preliminary intervention experiment using age-related IgG glycan signatures to evaluate

their potential effects on aging-related phenotypes (Fig. 6). Although the sample size was limited, we observed consistent trends across several key indicators, including body weight, inflammatory cytokines, and tissue senescence, which aligned with glycan profile shifts. These results suggest possible biological relevance but must be interpreted with caution due to the small number of animals involved.

In summary, this study highlights the downregulation of GP3 (F(6)A2B) and the upregulation of GP8 (F(6)A2G2) during the aging process in C57BL/6 mice and elucidates the role of CR in modulating these glycan changes as part of its antiaging effects. We also demonstrated the potential of bisected glycan and digalactosylated glycan as biomarkers of aging and health. By establishing a glycan age prediction model, abGlycoAge, this study quantified the biological relevance of glycosylation in the aging process. Furthermore, the application of absolute quantification techniques facilitated the precise detection of alterations in low-abundance glycans and improved the feasibility of using discovered, specifically changed glycans as practical biomarkers. In addition, our findings indicate a potential novel antiaging strategy: precise modulation of GP3 and GP8 on IgG through glycoengineering. Moreover, our investigation of IgG-Ny treatment revealed its potential for reversing aging, with high-dose IgG-Ny not only failing to promote aging but also effectively alleviating aging-related physiological decline, reducing aging-related inflammatory factors, and improving the state of organ senescence, particularly in the brain, kidney, and lung. These results underscore the dose-dependent and organ-specific effects of IgG-Ny treatment, suggesting its potential as a targeted antiaging intervention. Together, these findings not only deepen our understanding of glycan changes during aging but also support the development of new antiaging intervention strategies and predictive biomarkers.

CRediT authorship contribution statement

Huijuan Zhao: Writing – original draft, Visualization, Formal analysis, Data curation. **Jiteng Fan:** Writing – original draft, Data curation. **Jing Han:** Data curation. **Wenjun Qin:** Methodology. **Jichen Sha:** Data curation. **Weilong Zhang:** Investigation, Data curation. **Yong Gu:** Data curation. **Xiaonan Ma:** Investigation. **Jianxin Gu:** Project administration, Conceptualization. **Shifang Ren:** Writing – review & editing, Methodology, Conceptualization.

Declaration of competing interest

The authors declare that they have no known competing financial interests or personal relationships that could have appeared to influence the work reported in this paper.

Acknowledgments

We thank Prof. Tiehai Li from the Shanghai Institute of Materia Medica, Chinese Academy of Sciences, China, for his support in supplying the GP3 and GP8 *N*-glycan external standards.

This work was supported by grants from the National Key Research and Development Program of China (2022YFC3400800) and the National Natural Science Foundation of China (92478201, 32071276, and 32201046). The graphical study design was drawn in FigDraw.

Appendix A. Supplementary data

Supplementary data to this article can be found online at <https://doi.org/10.1016/j.eng.2025.07.042>.

References

- [1] Campisi J, Kapahi P, Lithgow GJ, Melov S, Newman JC, Verdin E. From discoveries in ageing research to therapeutics for healthy ageing. *Nature* 2019;571(7764):183–92.
- [2] Sayed N, Huang Y, Nguyen K, Krejciwo-Rajaniemi Z, Grawe AP, Gao T, et al. An inflammatory aging clock (iAge) based on deep learning tracks multimorbidity, immunosenescence, frailty and cardiovascular aging. *Nat Aging* 2021;1(7):598–615.
- [3] Liu Z, Liang Q, Ren Y, Guo C, Ge X, Wang L, et al. Immunosenescence: molecular mechanisms and diseases. *Signal Transduct Target Ther* 2023;8(1):200.
- [4] Hematianlarki M, Nimmerjahn F. Immunomodulatory and anti-inflammatory properties of immunoglobulin G antibodies. *Immunol Rev* 2024;328(1):372–86.
- [5] Schjoldager KT, Narimatsu Y, Joshi HJ, Clausen H. Global view of human protein glycosylation pathways and functions. *Nat Rev Mol Cell Biol* 2020;21(12):729–49.
- [6] Xu X, Peng Q, Jiang X, Tan S, Yang W, Han Y, et al. Altered glycosylation in cancer: molecular functions and therapeutic potential. *Cancer Commun* 2024;44(11):1316–36.
- [7] Wang W. Can DNA be glycosylated? *Engineering*. In press.
- [8] Shields RL, Lai J, Keck R, O'Connell LY, Hong K, Meng YG, et al. Lack of fucose on human IgG1 N-linked oligosaccharide improves binding to human FcγRIII and antibody-dependent cellular toxicity. *J Biol Chem* 2002;277(30):26733–40.
- [9] Shibata-Koyama M, Iida S, Misaka H, Mori K, Yano K, Shitara K, et al. Nonfucosylated rituximab potentiates human neutrophil phagocytosis through its high binding for FcγRIIIb and MHC class II expression on the phagocytotic neutrophils. *Exp Hematol* 2009;37(3):309–21.
- [10] Walters H. IgG is an early driver of aging. *Nat Aging* 2024;4(3):279.
- [11] Yu L, Wan Q, Liu Q, Fan Y, Zhou Q, Skowronski AA, et al. IgG is an aging factor that drives adipose tissue fibrosis and metabolic decline. *Cell Metab* 2024;36(4):793–807.e5.
- [12] Parekh R, Roitt I, Isenberg D, Dwek R, Rademacher T. Age-related galactosylation of the N-linked oligosaccharides of human serum IgG. *J Exp Med* 1988;167(5):1731–6.
- [13] Yamada E, Tsukamoto Y, Sasaki R, Yagyu K, Takahashi N. Structural changes of immunoglobulin G oligosaccharides with age in healthy human serum. *Glycoconj J* 1997;14(3):401–5.
- [14] Kristic J, Vuckovic F, Menni C, Klaric L, Keser T, Beccheli I, et al. Glycans are a novel biomarker of chronological and biological ages. *J Gerontol Biol Sci Med Sci* 2014;69(7):779–89.
- [15] Yu X, Wang Y, Kristic J, Dong J, Chu X, Ge S, et al. Profiling IgG N-glycans as potential biomarker of chronological and biological ages: a community-based study in a Han Chinese population. *Medicine* 2016;95(28):e4112.
- [16] Sun W, Jian X, Zhang J, Meng X, Wang H, Zheng D, et al. The causality between human immunoglobulin G (IgG) N-glycosylation and aging: a Mendelian randomization study. *Molecules* 2024;29(6):1281.
- [17] Greto VL, Cvetko A, Stambuk T, Dempster NJ, Kifer D, Deris H, et al. Extensive weight loss reduces glycan age by altering IgG N-glycosylation. *Int J Obes* 2021;45(7):1521–31.
- [18] Mijakovac A, Frkatic A, Hanic M, Ivok J, Kavur MM, Pucic-Bakovic M, et al. Heritability of the glycan clock of biological age. *Front Cell Dev Biol* 2022;10:982609.
- [19] Mehta N, Porterfield M, Struwe WB, Heiss C, Azadi P, Rudd PM, et al. Mass spectrometric quantification of N-linked glycans by reference to exogenous standards. *J Proteome Res* 2016;15(9):2969–80.
- [20] Simpson J, Zhang Q, Ozaeta P, Aboleneen H. A specific method for the measurement of cyclosporin a in human whole blood by liquid chromatography-tandem mass spectrometry. *Ther Drug Monit* 1998;20(3):294–300.
- [21] Perkins GL, Slater ED, Sanders GK, Prichard JG. Serum tumor markers. *Am Fam Physician* 2003;68:1075–82.
- [22] Groeneveld G, de Puit M, Bley S, Bradshaw R, Francese S. Detection and mapping of illicit drugs and their metabolites in fingerprints by MALDI MS and compatibility with forensic techniques. *Sci Rep* 2015;5(1):11716.
- [23] Nakano M, Uemura O, Honda M, Ito T, Nakajima Y, Saitoh S. Development of tandem mass spectrometry-based creatinine measurement using dried blood spot for newborn mass screening. *Pediatr Res* 2017;82(2):237–43.
- [24] Echeverria B, Etxebarria J, Ruiz N, Hernandez A, Calvo J, Habeger M, et al. Chemo-enzymatic synthesis of (13)C labeled complex N-glycans as internal standards for the absolute glycan quantification by mass spectrometry. *Anal Chem* 2015;87(22):11460–7.
- [25] Delafield DG, Li L. Recent advances in analytical approaches for glycan and glycopeptide quantitation. *Mol Cell Proteomics* 2021;20:100054.
- [26] Kailemia MJ, Ruhaak LR, Lebrilla CB, Amster IJ. Oligosaccharide analysis by mass spectrometry: a review of recent developments. *Anal Chem* 2014;86(1):196–212.
- [27] Qin W, Zhang Z, Qin R, Han J, Zhao R, Gu Y, et al. Providing Bionic Glycome as internal standards by glycan reducing and isotope labeling for reliable and simple quantitation of N-glycome based on MALDI-MS. *Anal Chim Acta* 2019;1081:112–9.
- [28] Han J, Pan Y, Gu Y, Xu X, Zhao R, Sha J, et al. Profiling of IgG N-glycome during mouse aging: fucosylated diantennary glycans containing one Neu5Gc-linked LacNAc are associated with age. *J Proteomics* 2020;229:103966.
- [29] Fan J, Sha J, Chang S, Zhao H, Niu X, Gu Y, et al. Generalized low levels of serum N-glycans associate with better health status. *Aging Cell* 2023;22(7):e13855.
- [30] Reiding KR, Blank D, Kuijper DM, Deelder AM, Wuhrer M. High-throughput profiling of protein N-glycosylation by MALDI-TOF-MS employing linkage-specific sialic acid esterification. *Anal Chem* 2014;86(12):5784–93.
- [31] Love MI, Huber W, Anders S. Moderated estimation of fold change and dispersion for RNA-seq data with DESeq2. *Genome Biol* 2014;15(12):550.
- [32] Subramanian A, Tamayo P, Mootha VK, Mukherjee S, Ebert BL, Gillette MA, et al. Gene set enrichment analysis: a knowledge-based approach for interpreting genome-wide expression profiles. *Proc Natl Acad Sci USA* 2005;102(43):15545–50.
- [33] Blake JA, Baldarelli R, Kadin JA, Richardson JE, Smith CL, Bult CJ, et al. Mouse genome database (MGD): knowledgebase for mouse-human comparative biology. *Nucleic Acids Res* 2021;49(D1):D981–7.
- [34] Lauc G, Huffman JE, Pucic M, Zgaga L, Adamczyk B, Muzinic A, et al. Loci associated with N-glycosylation of human immunoglobulin G show pleiotropy with autoimmune diseases and hematological cancers. *PLoS Genet* 2013;9(1):e1003225.
- [35] Frkatic A, Hodzic A, Mijakovac A, Miskec K, Nostaeva A, Sharapov SZ, Landini A, et al. Mapping of the gene network that regulates glycan clock of ageing. *Aging* 2023;15(24):14509–52.
- [36] Mijakovac A, Juric J, Kohrt WM, Kristic J, Kifer D, Gavin KM, et al. Effects of estradiol on immunoglobulin G glycosylation: mapping of the downstream signaling mechanism. *Front Immunol* 2021;12:680227.
- [37] Mijakovac A, Miskec K, Kristic J, Bockor VV, Tadic V, Boskovic M, et al. A transient expression system with stably integrated CRISPR-cas9 fusions for regulation of genes involved in immunoglobulin G glycosylation. *CRISPR J* 2022;5(2):237–53.
- [38] Shadrina AS, Zlobin AS, Zaytseva OO, Klaric L, Sharapov SZ, Pakhomov ED, et al. Multivariate genome-wide analysis of immunoglobulin G N-glycosylation identifies new loci pleiotropic with immune function. *Hum Mol Genet* 2021;30(13):1259–70.
- [39] Foell J, Strahotin S, O'Neil SP, McCausland MM, Suwyn C, Haber M, et al. CD137 costimulatory T cell receptor engagement reverses acute disease in lupus-prone NZB × NZW F₁ mice. *J Clin Invest* 2003;111(10):1505–18.
- [40] Liu Y, Shen J, Fortmann SD, Wang J, Vestweber D, Campochiaro PA. Reversible retinal vessel closure from VEGF-induced leukocyte plugging. *JCI Insight* 2017;2(18):e95530.
- [41] Kumagai S, Togashi Y, Kamada T, Sugiyama E, Nishinakamura H, Takeuchi Y, et al. The PD-1 expression balance between effector and regulatory T cells predicts the clinical efficacy of PD-1 blockade therapies. *Nat Immunol* 2020;21(11):1346–58.
- [42] Zaytseva OO, Jansen BC, Hanic M, Mrcela M, Razdorov G, Stojkovic R, et al. MigGGly (mouse IgG glycosylation analysis)—a high-throughput method for studying Fc-linked IgG N-glycosylation in mice with nanoUPLC-ESI-MS. *Sci Rep* 2018;8(1):13688.
- [43] Ma S, Ji Z, Zhang B, Geng L, Cai Y, Nie C, et al. Spatial transcriptomic landscape unveils immunoglobulin-associated senescence as a hallmark of aging. *Cell* 2024;187(24):7025–44.e34.
- [44] Trbojevic-Akmacic I, Lageveen-Kammeijer GSM, Heijs B, Petrovic T, Deris H, Wuhrer M, et al. High-throughput glycomic methods. *Chem Rev* 2022;122(20):15865–913.
- [45] Yang K, Li X, Lai M, Zhao W, Song W, Chen S, et al. Ablation of *ST6Gal-I* downregulates BACE1 expression and suppresses production of Aβ₄₂ plaques in Alzheimer's disease. *Engineering*. In press.
- [46] Giron LB, Liu Q, Adeniji OS, Yin X, Kannan T, Ding J, et al. Immunoglobulin G N-glycan markers of accelerated biological aging during chronic HIV infection. *Nat Commun* 2024;15(1):3035.
- [47] Moh ES, Thaysen-Andersen M, Packer NH. Relative versus absolute quantitation in disease glycomics. *Proteomics Clin Appl* 2015;9(3–4):368–82.
- [48] Liu X, Meng Y, Fu B, Song H, Gu B, Zhang Y, et al. GlycoPro: a high-throughput sample-processing platform for multi-glycosylation-omics analysis. *Engineering*. In press.
- [49] Zuniga-Banuelos FJ, Hoffmann M, Reichl U, Rapp E. New avenues for human blood plasma biomarker discovery via improved in-depth analysis of the low-abundant N-glycoproteome. *Engineering*. In press.
- [50] Wu Z, Guo Z, Zheng Y, Wang Y, Zhang H, Pan H, et al. IgG N-glycosylation cardiovascular age tracks cardiovascular risk beyond calendar age. *Engineering* 2023;26:99–107.
- [51] Ercan A, Kohrt WM, Cui J, Deane KD, Pezer M, Yu EW, et al. Estrogens regulate glycosylation of IgG in women and men. *JCI Insight* 2017;2(4):e89703.